JOURNAL OF GEOPHYSICAL RESEARCH, VOL. 107, NO. D13, 4184, 10.1029/2001JD001178, 2002.

Tropical ozone as an indicator of deep convection

Ian Folkins and Christopher Braun
Department of Physics and Atmospheric Science, Dalhousie University, Halifax, Nova Scotia, Canada

Anne M. Thompson and Jacquelyn Witte
NASA/Goddard, Atmospheric Chemistry and Dynamics Branch, Greenbelt, Maryland, USA

Received 1 August 2001; revised 2 November 2001; accepted 6 November 2001; published 12 July 2002.

[1] The climatological ozone profile in the tropics is shaped like an "S," with a minimum at the surface, a maximum at 330 K (~6.5 km), another minimum at 345 K (~11.2 km), and a subsequent increase toward the tropopause. These features can be reproduced by a very simple model whose only free parameter is the mean ozone mixing ratio of air detraining from deep convective clouds. To first order, the climatological ozone profile in the tropics arises from a balance between vertical advection, deep convection, and chemistry. The 345 K ozone minimum is coincident with a lapse rate minimum. Both minima are associated with a large increase in convective outflow at 345 K followed by a quasi-exponential decrease. The increase in ozone above 345 K is caused mainly by decreased injection of low-ozone air from the boundary layer. The model tends to underestimate ozone between 340 and 365 K (~9–15 km). This is most likely due either to an underestimate by the model of in situ ozone production or to eddy transport of ozone from the lowermost stratosphere into the upper tropical troposphere across the subtropical jet. The magnitudes of both these processes are poorly constrained by measurements. In the case of ozone production this is mainly due to a lack of measurements of HO_x precursors such as acetone and CH_3OOH between 11 and 16 km. *INDEX TERMS:* 0368 Atmospheric Composition and Structure: Troposphere—constituent transport and chemistry; 3314 Meteorology and Atmospheric Dynamics: Convective processes; 0365 Atmospheric Composition and Structure: Troposphere—composition and chemistry; 3374 Meteorology and Atmospheric Dynamics: Tropical meteorology; *KEYWORDS:* ozone, convection, tropics, troposphere, detrainment

1. Introduction

[2] The tropical troposphere is often thought of as being well mixed by deep convection up to the cold point (or lapse rate) tropopause. Recently, however, there have been attempts to describe the interface between the tropical troposphere and the stratosphere from a more statistical point of view. Unfortunately, it is very difficult to directly measure the vertical variation of convective outflow in the tropics. Investigators have therefore tried to infer convective outflow from a variety of indirect methods, including arrays of radiosondes [*Yanai et al.*, 1973], chemical tracers such as CFCs and N_2O [*Tuck et al.*, 1997], ozone [*Folkins et al.*, 1999], the vertical variation of clear sky radiative heating rates [*Folkins et al.*, 2000; *Folkins*, 2002], cloud imagery [*Highwood and Hoskins*, 1998; *Gettelman et al.*, 2002], or variations in both ozone and carbon monoxide [*Dessler*, 2002]. Ozone is particularly useful for this purpose because its chemical lifetime is comparable with the timescale for overturning within the Hadley circulation and because there now exists a database sufficiently long for climatological analyses [*Thompson et al.*, 2002].

[3] Future changes in ozone may give rise to important climate feedbacks. In the tropics, ozone is expected to evolve in response to both changes in in situ production, arising from changes in surface emissions of CO and NO, and from changes in the vertical variation of convective outflow, anticipated from changes in sea surface temperatures. In the vicinity of the cold point tropopause, ozone plays an important role in the clear sky radiation budget, so that future changes in its vertical distribution are likely to have some impact on the evolution of cold point temperatures. These changes may also influence temperatures at the surface since the greenhouse forcing of ozone (on a per-molecule basis) is maximized near the cold point [*Lacis et al.*, 1990].

[4] Figure 1 shows the variation of ozone with potential temperature at several locations in the Southern Hemisphere Additional Ozonesondes (SHADOZ) data set [*Thompson et al.*, 2002]. With the exception of Kaashidhoo each of the profiles represents an annual climatology. The ozone profile at Kaashidhoo was obtained from ozonesondes launched between January and March 1999 from the Maldive Islands as part of the Indian Ocean Experiment (INDOEX) campaign [*Lelieveld et al.*, 2001]. Ozone is lowest at the sites most strongly associated with active marine convection, such as Samoa (14.2°S, 170.6°W), Fiji (18.1°S, 178.4°E), Kaashidhoo (5.0°N, 73.5°E), and to a lesser extent, San Cristóbal (0.9°S, 89.6°W) (in the eastern equatorial Pacific). Ozone is larger at locations associated with continental

0148-0227/02/2001JD001178

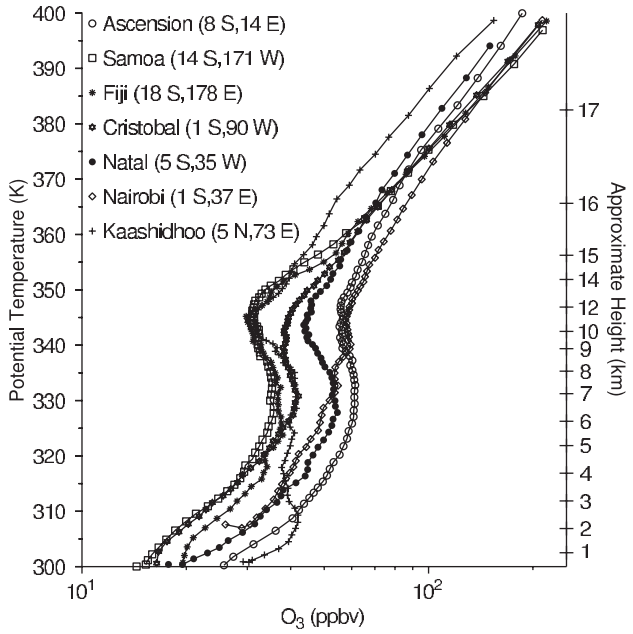

Figure 1. The mean annual dependence of ozone mixing ratio on potential temperature at Ascension (118), Samoa (175), Fiji (114), Cristóbal (131), Natal (68), Nairobi (132), and Kaashidhoo (53), where the number given in parentheses is the number of ozonesondes used at each location to construct the climatology. The Kaashidhoo profile is from ozonesondes launched during January–March. Latitude and longitude coordinates of each location are shown.

convection, such as Nairobi (1.3°S, 36.8°E) (Kenya), Natal (5.4°S, 35.4°W) (Brazil), and Ascension (8.0°S, 14.4°W) (between Brazil and Africa). The lower ozone mixing ratios above 355 K at Kaashidhoo probably reflect the fact that this profile represents a Northern Hemisphere winter climatology. Despite the regional variations in the troposphere, most of the profiles exhibit a common vertical S-shaped structure, with the lowest values found near the surface, a maximum near 330 K (~6.5 km), a minimum near 345 K (~11.2 km), and a subsequent increase toward stratospheric values.

[5] The factors that determine the vertical variation of ozone in the tropics can be grouped together into seven categories: (1) in situ production/destruction, (2) deep convective outflow, (3) vertical advection, (4) shallow convection, (5) eddy exchange with the midlatitudes/lowermost stratosphere, (6) convective downdrafts, and (7) vertical mixing near the tropical tropopause associated with convective overshooting [*Sherwood and Dessler*, 2001] and Kelvin waves [*Fujiwara et al.*, 1998]. We will argue in section 2 that deep convective outflow is largely restricted to altitudes above 345 K. Shallow convection refers to the mixing occurring along the sides of deep convective updrafts or that associated with shallow dissipating convective plumes. Vertical advection refers to the ozone tendency arising from the slow radiatively driven vertical motions in the tropics. These are ordinarily downward below 360 K (~15.2 km) and upward above 360 K [*Folkins*, 2002]. Given the climatological profiles shown in Figure 1, this tendency should be negative above 360 K, positive between 345 and 360 K, negative between 345 and 330 K, and positive below 330 K. The existence of eddy exchange with midlatitudes is most often revealed by the layers of high ozone/low relative humidity frequently observed in the tropical midtroposphere [*Danielsen et al.*, 1987]. Its existence at higher altitudes can be inferred from the onset of decreases in CFCs and N_2O well below the tropical tropopause [*Tuck et al.*, 1997].

[6] Figure 2 shows the characteristic dependence of the ozone tendency $(dO_3/dt)_{chem}$ on potential temperature in the tropics. The chemical tendency was generated by a model that was heavily constrained by aircraft measurements of ozone precursors. Its origin is discussed in more detail in section 4. The transition from lower tropospheric net ozone destruction to upper tropospheric net ozone production occurs at 330 K, near the bulge in the climatological ozone profiles shown in Figure 1. Ozone is destroyed near the surface at a rate of ~2–3 ppbv/day. Since ozone mixing ratios at the surface are typically 15–30 ppbv, the ozone lifetime near the surface is ~10 days, in agreement with previous estimates [e.g., *Thompson et al.*, 1993].

[7] It is sometimes thought that ozone increases in going from the troposphere to the stratosphere because of increased photolysis of molecular oxygen, the main source of ozone in the stratosphere. As shown in Figure 2, $(dO_3/dt)_{chem}$ does increase above 380 K (~16.8 km), and this increase is due to O_2 photolysis. It appears unlikely, however, that the increase in $(dO_3/dt)_{chem}$ above 380 K is responsible for the increases in ozone which start near

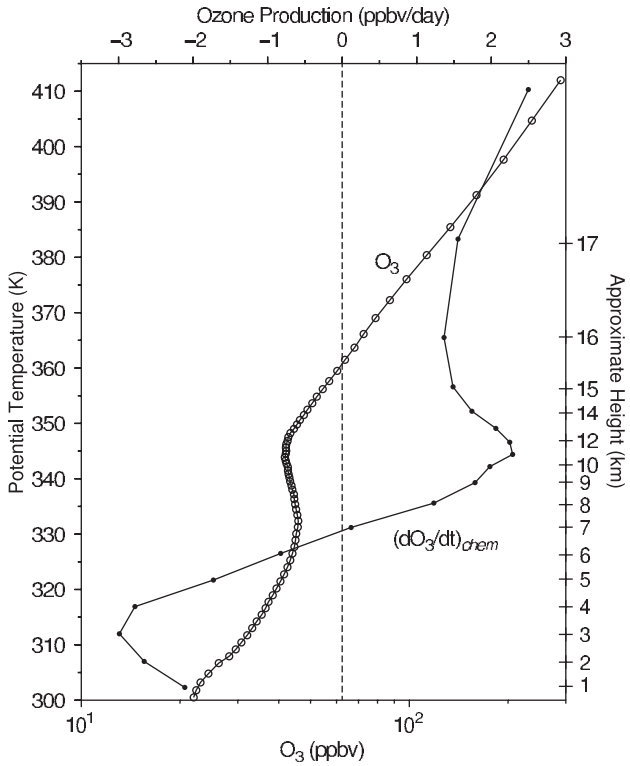

Figure 2. The curve in open circles is a mean annual tropical ozone climatology generated by averaging the ozonesondes used to make the climatologies shown in Figure 1. The curve in closed circles is the ozone tendency $(dO_3/dt)_{chem}$. Its construction is described in section 4.

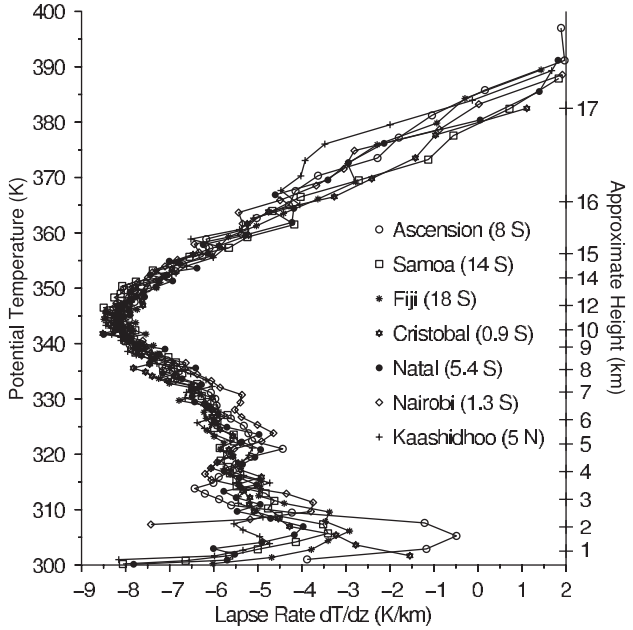

Figure 3. The dependence of lapse rate (dT/dz) on potential temperature at various tropical locations. There is a lapse rate minimum near 345 K at each location.

345 K (~11.2 km). It was therefore suggested that the positive ozone gradient in the upper tropical troposphere reflected a decrease in the deep convective pumping of ozone-depleted marine boundary layer air into the upper tropical troposphere [*Folkins et al.*, 1999]. This was supported by showing that the ozone increases were correlated with increases in lapse rate. This is also shown in Figure 3, which shows the lapse rate as a function of potential temperature at each of the seven locations as used in Figure 1. There is a well-defined 345 K lapse rate minimum at each location.

[8] In the first part of this paper the frequency of occurrence of air parcels with ozone mixing ratios characteristic of the boundary layer is used as a proxy for deep convective outflow. We show that this proxy is consistent with the rate of convective detrainment, as diagnosed from the vertical variation of clear sky radiative cooling rates. In the second part of the paper we show that the general characteristics of the tropical ozone profiles shown in Figure 1 can be captured by a very simple model.

2. Low Ozone As a Proxy for Deep Convection

[9] Between 345 and 360 K each of the seven terms in the ozone budget discussed in section 1 is likely to be positive except for the tendency associated with deep convection. The only region of the tropical troposphere able to generate ozone mixing ratios as low as 15, 20, or 25 ppbv is near the surface. An air parcel in the upper tropical troposphere with an ozone mixing ratio less than 15, 20, or 25 ppbv is therefore likely to be of recent boundary layer origin. Figure 4 shows the fraction of air parcels less than 15, 20, and 25 ppbv as a function of potential temperature. In addition to using ozonesondes from the SHADOZ locations shown in Figure 1, we also used 66 ozonesondes from Java (7.5°S, 112°E) and four ozonesondes from Christmas Island (2°N, 157°W). Each fraction has an upper tropospheric peak near 345 K, reaching values almost as high as those realized in the boundary layer. The double-peak structure implies that it is not possible to describe the vertical overturning associated with tropical deep convection as a diffusive process [e.g., *Chatfield and Crutzen*, 1984].

[10] In the tropics the net upward vertical mass flux associated with convective clouds is approximately balanced by clear sky subsidence associated with radiative cooling (provided the exchange with midlatitudes can be assumed small). The clear sky radiative mass flux can be expressed as

$$M_r(\theta) = \frac{\rho Q_r}{dT/dz + \Gamma_d}, \qquad (1)$$

where ρ is the density, Q_r is the clear sky radiative heating rate, dT/dz is the lapse rate, and Γ_d is the dry adiabatic lapse rate. The clear sky mass flux calculated from equation (1) is shown on the left-hand side of Figure 5. Q_r was calculated from a radiative transfer code using the δ four-stream method [*Fu and Liou*, 1992]. The input profiles of temperature, water vapor, and ozone were obtained from a combination of radiosonde and satellite measurements [*Folkins*, 2002]. To generate the 1999 25°S–25°N average shown in Figure 5, separate calculations of $M_r(\theta)$ were carried out for each 5° latitude bin from 25°S to 25°N and for each month of 1999.

[11] The right-hand side of Figure 5 shows $dM_r(\theta)/d\theta$, the rate of mass outflow between two isentropic surfaces associated with detrainment and entrainment of air from tropical clouds. It is quite small below 345 K, rapidly increases to a maximum value near 348 K (~12.5 km)

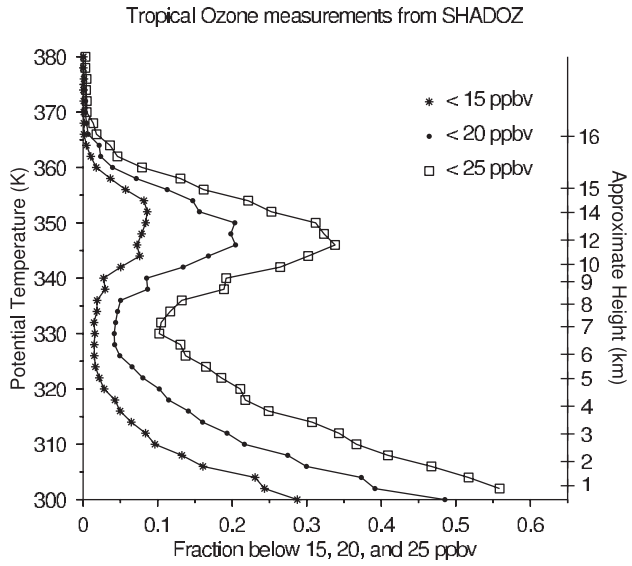

Figure 4. Each curve denotes the fraction of all ozone measurements at that potential temperature (2-K bins) whose ozone mixing ratio is less than 15, 20, or 25 ppbv. The fractions were produced using the 791 high-resolution ozonesondes used to construct the climatologies shown in Figure 1.

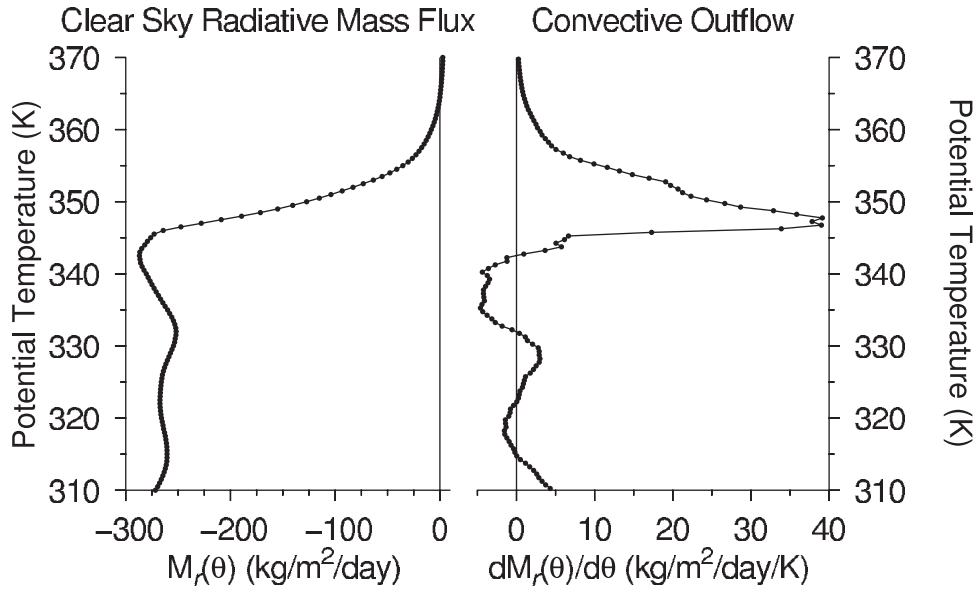

Figure 5. The plot on the left shows the clear sky radiative mass flux $M_r(\theta)$. The plot on the right shows the derivative of $M_r(\theta)$ with respect to potential temperature $dM_r(\theta)/d\theta$.

and then decreases in a quasi-exponential manner. We have argued that the rate of this decrease is controlled by the statistical distribution of pseudoequivalent potential temperature (θ_e) in the convective boundary layer (CBL) [*Folkins et al.*, 2000; *Folkins*, 2002]. The rapid increase in convective outflow at 345 K corresponds to the value of θ_e, at which the convective available potential energy of air parcels near the surface becomes positive.

[12] The rate of detrainment from convective clouds can be inferred from $M_r(\theta)$, provided the detrainment rate is assumed to be much larger than the entrainment rate. This approximation is probably reasonably accurate in the upper tropical troposphere. The detrainment rate $d(\theta)$ is then given by the vertical derivative of $M_r(\theta)$ with respect to pressure and is multiplied by g (i.e., the change in the mass flux between the top and bottom of a layer divided by mass of the layer).

$$d(\theta) = (g)\frac{dM_r(\theta)}{dp} \tag{2}$$

[13] Figure 6 shows the vertical variation of $d(\theta)$. It decreases quite rapidly above 354 K (~14 km) [*Folkins et al.*, 1999]. The detrainment decreases less rapidly with potential temperature than does $dM_r(\theta)/d\theta$ because the mass between potential temperature surfaces tends to diminish with height. The reciprocal of $d(\theta)$ can be interpreted as τ_{conv}, the timescale with which ambient air in the upper tropical troposphere is replaced by air detraining from convective clouds. As $d(\theta)$ decreases from a maximum of 0.38 d^{-1} at 348 K (~12.5 km), to 0.01 d^{-1} at 368 K (~16.0 km), the convective replacement timescale τ_{conv} increases from 2.6 to 100 days. A diagnosis of τ_{conv} from the vertical variation of O_3 and CO has suggested somewhat larger detrainment rates above 365 K [*Dessler*, 2002].

[14] The plot with open circles in Figure 6 shows the fraction of air parcels having ozone less than 25 ppbv. Between 345 K (~11.2 km) and 370 K (~16.2 km) this fraction and the detrainment rate decrease with potential temperature in a remarkably similar manner. This is also true if one uses an ozone threshold of 20 or 15 ppbv.

[15] The dependence of $d(\theta)$ on potential temperature is quite sensitive to the latitude range over which $M_r(\theta)$ is defined [*Folkins*, 2002]. If $d(\theta)$ is defined over a latitude range closer to the equator, it will peak at a larger value

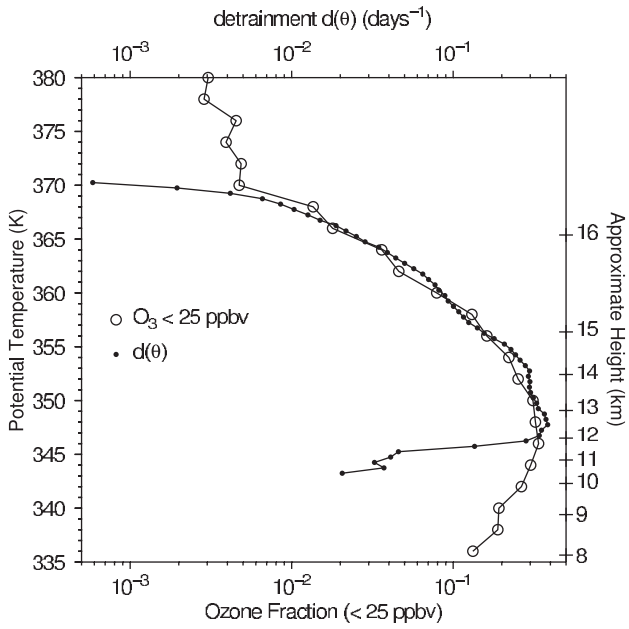

Figure 6. The curve with closed circles is $d(\theta)$, calculated from equation (1). The curve with open circles is the fraction of air parcels whose ozone mixing ratio is <25 ppbv.

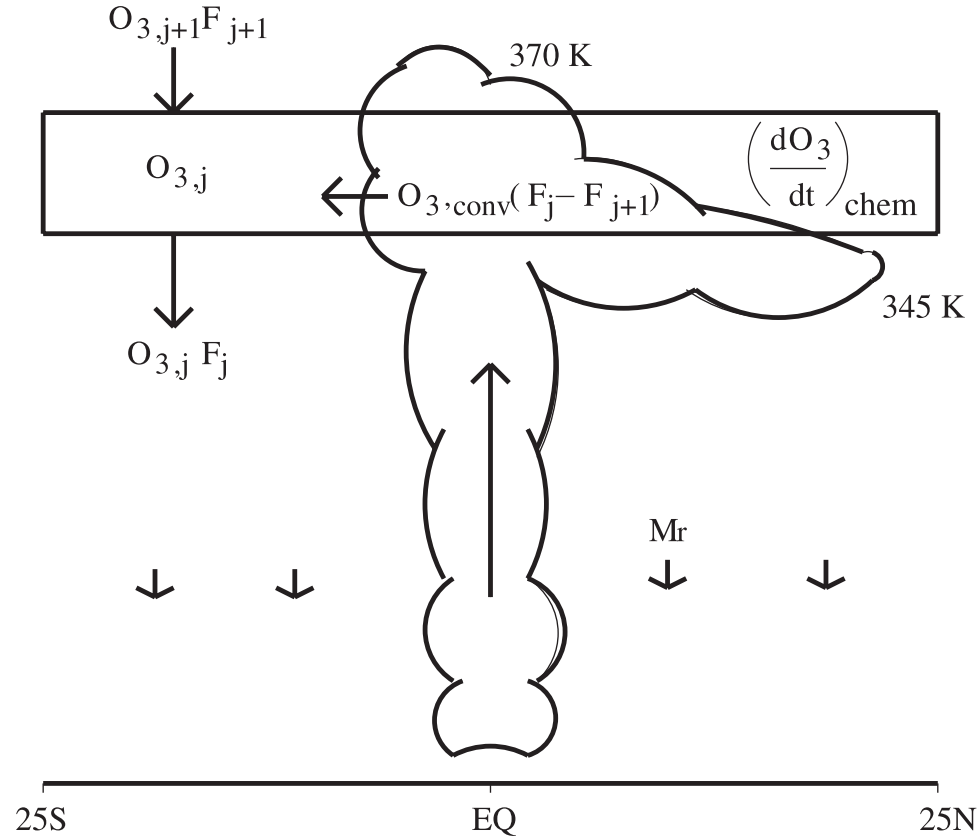

Figure 7. This figure shows the forcings used to generate the model ozone profile. The vertical dimension of the box shown is highly exaggerated. The convective forcing on the local ozone mixing ratio is largely restricted to a detrainment layer between 345 K (∼11.2 km) and 370 K (∼16.2 km).

and subsequently decrease more rapidly with potential temperature.

3. Simple Model of Tropical Ozone

[16] In this section we describe a simple model intended to investigate the possibility that the 345 K (∼11.2 km) ozone minimum is caused by a rapid increase in tropical deep convective outflow, as suggested by Figure 6. The model extends from 305 to 400 K in 1-K increments. Let N_j be the number of molecules in box j, and let $O_{3,j}$ be the ozone mixing ratio in box j. The number density flux between box $j-1$ and j is F_j (positive for upward, negative for downward). F_j is calculated from the clear sky radiative mass fluxes shown in Figure 5. Suppose that F_j and F_{j+1} are both downward and that F_j is larger than F_{j+1}, so that there is a larger flux out the bottom of a box than coming in from the top. We will assume that this divergence is balanced by a convective flux ($F_{j+1} - F_j$) and that this incoming flux can be characterized by a convective ozone mixing ratio $O_{3,\mathrm{conv}}$. If each box has unit area, the rate of change of $O_{3,j}$ is given by

$$\frac{dO_{3,j}}{dt} = \frac{1}{N_j}\left[-F_{j+1}O_{3,j+1} + F_jO_{3,j} + \left(F_{j+1} - F_j\right)O_{3,\mathrm{conv}}\right] + \left(\frac{dO_{3,j}}{dt}\right)_{\mathrm{chem}}. \quad (3)$$

This can be rewritten as

$$\frac{dO_{3,j}}{dt} = -\left(O_{3,j+1} - O_{3,j}\right)\frac{F_{j+1}}{N_j} + \left(O_{3,\mathrm{conv}} - O_{3,j}\right)\frac{\left(F_{j+1} - F_j\right)}{N_j} + \left(\frac{dO_{3,j}}{dt}\right)_{\mathrm{chem}}. \quad (4)$$

We will refer to the first term on the right as the vertical advective tendency. It is proportional to the difference between the ozone mixing ratio of the flux entering the box from above and the local ozone mixing ratio. The second term on the right will be referred to as the convective tendency. It scales with the difference between the ozone mixing ratio of the convected air and the local ozone mixing ratio. With these definitions, equation (4) can be rewritten as

$$\frac{dO_{3,j}}{dt} = \left(\frac{dO_{3,j}}{dt}\right)_{\mathrm{adv}} + \left(\frac{dO_{3,j}}{dt}\right)_{\mathrm{conv}} + \left(\frac{dO_{3,j}}{dt}\right)_{\mathrm{chem}}. \quad (5)$$

In the case that $F_j < 0$ and $F_{j+1} > 0$ (both fluxes are leaving the box) the vertical advective flux will be zero, but the convective flux can be expressed in a similar manner. In the case that $F_j > 0$ and $F_{j+1} < 0$ (both fluxes are entering the box) the convective flux is zero, but there is assumed to be a sideways ozone flux leaving box, given by $O_{3,j}(F_j - F_{j+1})$. The vertical advective flux can then be expressed as

$$\left(\frac{dO_{3,j}}{dt}\right)_{\mathrm{adv}} = \left(O_{3,j-1} - O_{3,j}\right)\frac{F_j}{N_j} - \left(O_{3,j+1} - O_{3,j}\right)\frac{F_{j+1}}{N_j}. \quad (6)$$

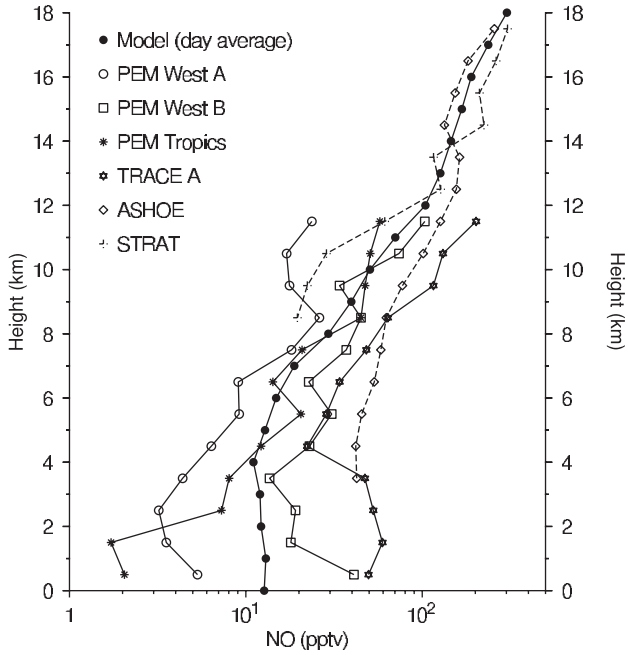

Figure 8. Climatological profiles of NO (30°S–30°N, with (SZA) < 60°) from various field campaigns. Day average NO mixing ratios from the model are shown as solid circles.

Other combinations of upward and downward fluxes can be handled in a similar way. An outline of the model is given in Figure 7.

[17] The N_j for each box was obtained from the 25°S–25°N pressure and temperature climatologies used to calculate $M_r(\theta)$. The only parameter in the model is $O_{3,conv}$. It is intended to represent the mean ozone mixing ratio of air detraining from deep convective systems in the tropics. Figure 1 shows that the climatological ozone mixing ratio at the surface varies from 15 to 30 ppbv. This should be adjusted upward because air will enter convective systems from throughout the CBL, or up to 800 mb (~307 K), and because entrainment of midtropospheric air during convection will increase $O_{3,conv}$. We therefore set $O_{3,conv}$ = 25 ppbv. The model is initialized with a uniform ozone mixing ratio of 10 ppbv and is then run for 200 days, sufficiently long for the ozone profile to reach steady state. The time step was 0.1 days.

4. Chemical Model

[18] The chemical tendency was implemented in the model in the form

$$\left(\frac{dO_3}{dt}\right)_{chem} = P - L[O_3], \tag{7}$$

so that the chemical tendency interacted with the ozone mixing ratio of the model [O_3] via the first-order loss. The production (P) and loss (L) were determined by a separate chemical model, which extended from 0 to 20 km. NO_x mixing ratios in the model were prescribed from a combination of measurements from the Global Tropospheric Experiment (GTE) missions below 12 km and from the Stratospheric Tracers of Atmospheric Transport (STRAT) and Airborne Southern Hemisphere Experiment/Measurements for Assessing the Effects of Stratospheric Aircraft (ASHOE/MAESA) campaigns above 12 km. Figure 8 shows the day average NO mixing ratio of the model, as well as 30°S–30°N NO climatologies (SZA < 60°) from several GTE missions, as well as STRAT and ASHOE/MAESA. Tropical STRAT and ASHOE/MAESA measurements below 15 km come mainly from ascents and descents based in Fiji and Hawaii. While the Pacific Exploratory Mission (PEM) West A, PEM West B, and PEM Tropics campaigns took place mainly over the Pacific, Transport and Atmospheric Chemistry Near the Equator—Atlantic (TRACE A) took place mainly over Africa. The larger NO mixing ratios over Africa are probably partially responsible for some of the regional variations in O_3 shown in Figure 1.

[19] Methyl hydroperoxide (CH_3OOH) mixing ratios in the upper tropical troposphere are typically several times larger than those predicted by steady state photochemical models [*Jacob et al.*, 1996]. This is probably caused by the convective injection of CH_3OOH-rich air from the boundary layer, where it can significantly increase HO_x concentrations [*Jaeglé et al.*, 1997] and ozone production [*Prather and Jacob*, 1997; *Folkins et al.*, 1998]. Below 12 km we fixed CH_3OOH mixing ratios using a climatology compiled from the GTE measurements. Above 16 km we used the model to calculate CH_3OOH. Between 12 and 16 km we

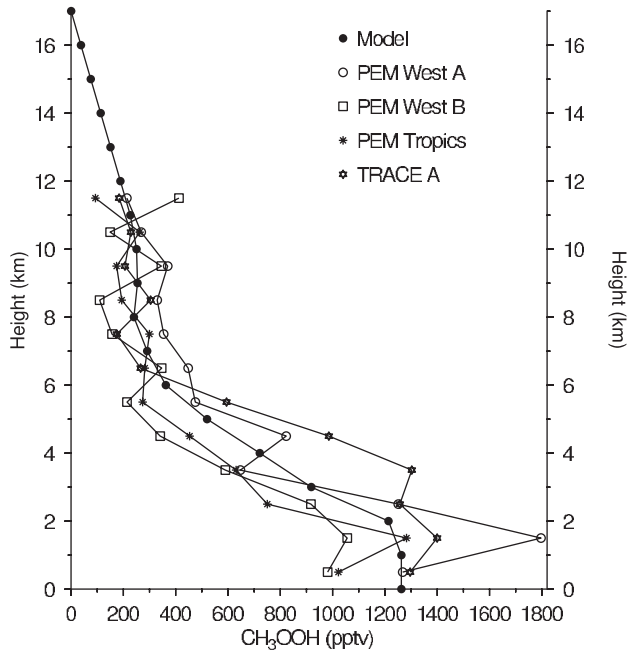

Figure 9. Climatological profiles of CH_3OOH (30°S–30°N) from various field campaigns. CH_3OOH mixing ratios from the model are shown as solid circles. Between 12 and 16 km, model values were specified by linear interpolation between the Global Tropospheric Experiment (GTE) average and the local photochemical steady state value. It is likely that the convective enhancement in CH_3OOH extends up to 14 km, above which $d(\theta)$ drops off rapidly.

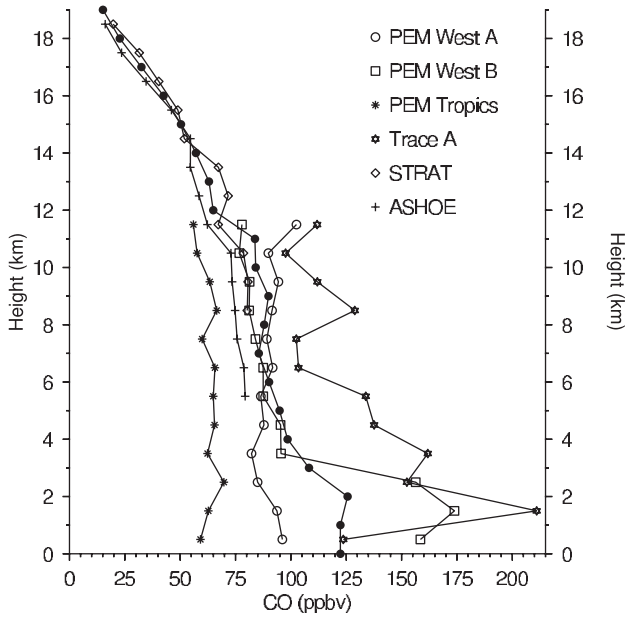

Figure 10. Climatological profiles of CO (30°S–30°N) from various field campaigns. CO mixing ratios from the model are shown as solid circles.

used linear interpolation between the GTE and model values. Model and GTE profiles of CH_3OOH are shown in Figure 9.

[20] The mixing ratio of carbon monoxide (CO) was also prescribed from a climatology of GTE, STRAT, and ASHOE/MAESA measurements. This is shown in Figure 10.

[21] Acetone is an important source of HO_x in the upper troposphere [*Singh et al.*, 1995; *McKeen et al.*, 1997; *Folkins et al.*, 1997; *Wennberg et al.*, 1998]. Below 12 km the model climatology was compiled from PEM West B and TRACE A measurements. Above 12 km we used an observed correlation between acetone and CO [*McKeen et al.*, 1997]. The model and GTE profiles are shown in Figure 11.

[22] The main chemical source of ozone in the upper troposphere is the reaction of NO with HO_2. Figure 12 shows the vertical profile of daytime average HO_2 in the model. Also shown are 30°S–30°N climatologies of HO_2 (SZA < 60°) from the STRAT and ASHOE/MAESA campaigns and the mean SZA as a function of height for the STRAT and ASHOE/MAESA HO_2 measurements.

[23] The mixing ratio of CH_4 in the model was fixed at 1.7 ppmv. Water vapor was prescribed from a radiosonde climatology [*Folkins*, 2002]. The mixing ratio of ozone was fixed by an ozonesonde climatology [*Logan*, 1999]. Peroxy acetyl nitrate (PAN) was fixed by a GTE climatology below 12 km and was linearly interpolated to zero at 18 km. It played no role in the chemistry other than to sequester NO_y. The mixing ratio of NO_y was fixed by STRAT and ASHOE/MAESA measurements above 5 km and was fixed at 400 pptv below 5 km. Since NO_x and PAN were fixed, the balance of NO_y was made up of HNO_3 and HO_2NO_2. H_2O_2 was fixed by a GTE climatology below 12 km and was otherwise calculated by the model. We used the phodis package to calculate photolysis rates (A. Kylling, unpublished data, 1995, available by anonymous ftp to kaja.gi.alaska.edu, cd pub/arve). The model was run in perpetual 21 March conditions (overhead Sun at the equator) for a latitude 15° from the equator. The model used standard HO_x-NO_x-CH_4 chemistry with additional HO_x production from acetone. The model had a total of 10 fixed species, 19 calculated species, and 16 photolysis rates.

[24] Figure 2 shows that there was a peak in $(dO_3/dt)_{chem}$ near 345 K (~11.2 km). While this peak may be realistic, and perhaps associated with a local maximum in convectively injected ozone precursors, it is produced in the model by a decrease above 11 km of HO_2, which arises from decreases in the HO_x precursors acetone (Figure 11) and CH_3OOH (Figure 9). Owing to a lack of measurements the variation of acetone and CH_3OOH above 11 km has been imposed in an ad hoc manner and may be inaccurate.

[25] The absence of acetone and CH_3OOH measurements between 11 and 15 km is one of several sources of error in our estimate of $(dO_3/dt)_{chem}$. Another source of error is that the dependence of the chemical tendency on ozone precursors is nonlinear, so that averaged profiles of NO, CO, etc., will not necessarily generate an accurate mean profile of $(dO_3/dt)_{chem}$. The profile shown in Figure 2 does, however, lie within the envelope of mean ozone production estimates obtained from the various GTE campaigns [*Schultz et al.*, 1999]. The zero in $(dO_3/dt)_{chem}$ near 6 km is a generic feature of these profiles and is associated with a decrease in the rate of ozone destruction from the $O^1D + H_2O$ reaction.

5. Model Results

[26] Figure 13 shows the vertical ozone profile predicted by the model together with the mean tropical SHADOZ profile. The model is quite successful at replicating the shape of the mean profile, including the surface minimum,

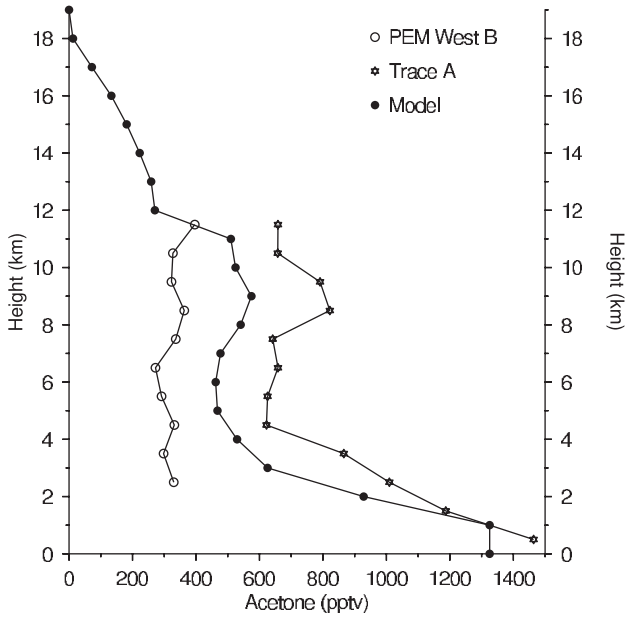

Figure 11. Climatological profiles of acetone (30°S–30°N) from two GTE field campaigns. Above 11 km, acetone in the model was obtained from a correlation with CO [*McKeen et al.*, 1997]. Unfortunately, the lack of acetone measurements above 11 km makes this extrapolation highly uncertain.

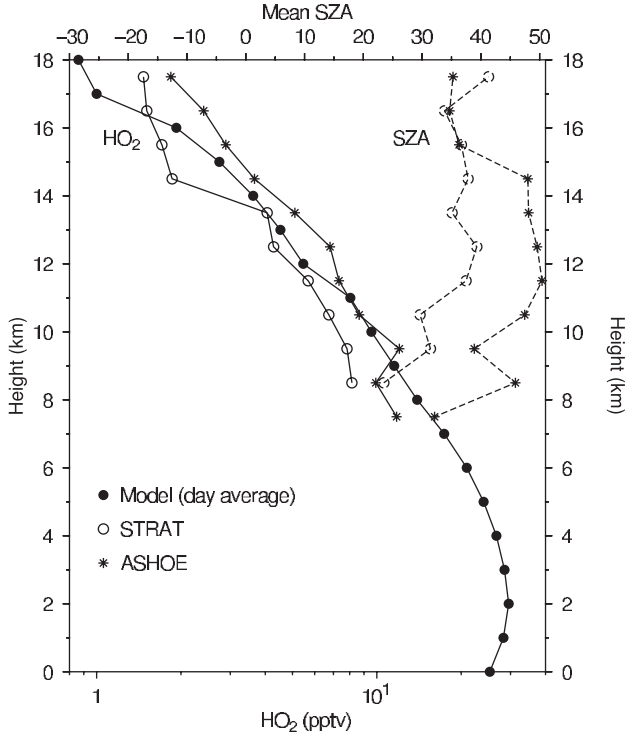

Figure 12. Climatological profiles of HO_2 (30°S–30°N) from Stratospheric Tracers of Atmospheric Transport (STRAT) and Airborne Southern Hemisphere Experiment/ Measurements for Assessing the Effects of Stratospheric Aircraft (ASHOE/MAESA). Day average HO_2 mixing ratios from the model are shown as closed circles. Also shown are the mean solar zenith angles corresponding to each of the STRAT and ASHOE/MAESA averages.

the 330 K peak, the 345 K minimum, and the increase above 345 K. The main failing of the model is that it underestimates observed ozone between 340 and 365 K (~9–15 km).

[27] Figure 14 shows the vertical variation of the vertical advective, convective, and chemical tendencies in the model, as defined in equations (3), (4), and (5). The convective tendency plays an important role in lowering ozone mixing ratios between 345 K (~11.2 km) and 370 K (~16.2 km). This negative tendency is balanced by the positive tendencies associated with vertical advection and in situ production. The convective tendency decreases with potential temperature above 348 K (~12.5 km) much less rapidly than does the detrainment rate $d(\theta)$ (shown in Figure 6). This is mainly because the convective tendency scales with $(O_{3,conv} - O_{3,j})$, which increases as the ambient ozone mixing ratio progressively increases.

[28] Figure 13 also shows the photochemical steady state (PSS) ozone mixing ratio of the model (i.e., with the convective and vertical advective forcings set to zero). The PSS profile approaches the climatology above 355 K as the detrainment rate decreases. Note that PSS ozone mixing ratios in the upper tropical troposphere are several hundred ppbv. This may be an overestimate of the real PSS value because the ozone production in equation (7) is specified independently of the ambient ozone mixing ratio. It does demonstrate, however, the power of convection in the upper tropical troposphere in "locking" ambient mixing ratios to a value near $O_{3,conv}$, which is much lower than the PSS value. It is important, however, to keep the dual nature of tropical convection in mind. Convection will almost always look like a negative tendency locally, but it does replenish the upper tropical troposphere with ozone precur-

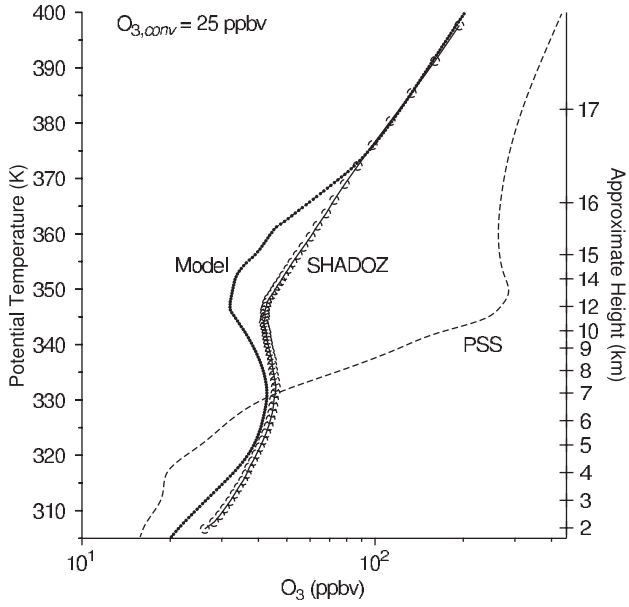

Figure 13. The ozone profile from the model together with the Southern Hemisphere Additional Ozonesondes (SHADOZ) climatology. Also shown is the photochemical steady state (PSS) ozone profile generated by the model chemical tendency.

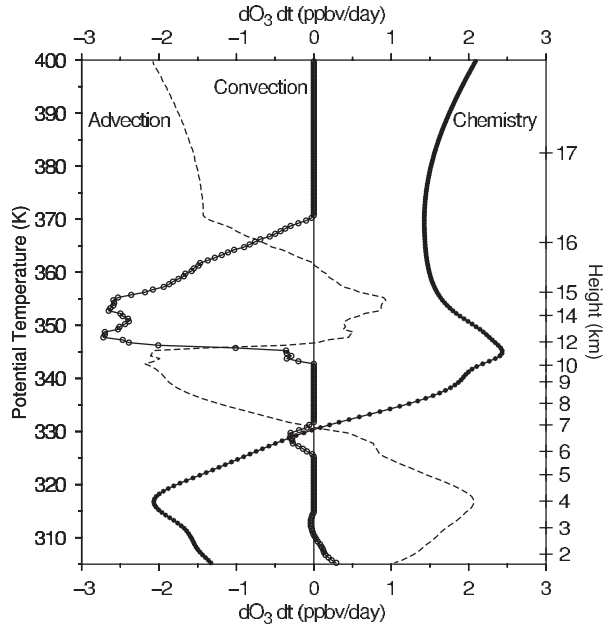

Figure 14. Vertical profiles of the vertical advective, convective, and chemical tendencies in the model. The small convective forcings near 310 and 330 K may not be physically significant.

sors, without which $(dO_3/dt)_{chem}$ and the PSS ozone mixing ratio would be much lower.

[29] The vanishing of the convective forcing at 370 K suggests that regional variations in O_3 (at least on θ surfaces) associated with near surface variations in ozone, ozone precursors, and convective frequency should be small above 370 K. This is roughly consistent with Figure 1. Above 370 K the mean ozone profile reflects a balance between vertical advection and chemical production [*Dessler et al.*, 1996]. This is also the case below 345 K. The increase in the mean ozone profile in descending from 345 to 330 K is driven by a combination of large scale descent and a positive chemical tendency, while the decrease below 330 K is associated with a change in sign of the chemical tendency, so that ozone mixing ratios now decrease as air subsides.

[30] Figure 15 shows the ozone profile generated by the model with $O_{3,conv}$ = 20 ppbv (probably representative of marine convection) and $O_{3,conv}$ = 30 ppbv (probably representative of continental convection). The value of $O_{3,conv}$ has little effect on the shape of the ozone profile. The $O_{3,conv}$ = 30 ppbv profile is, however, in better agreement with the SHADOZ climatology. Entrainment of midtropospheric air into deep convective clouds could account for a $O_{3,conv}$ larger than near surface ozone mixing ratios.

6. Eddy Transport

[31] The assumption that the tropics can be considered dynamically isolated from midlatitudes is probably one of the more serious deficiencies of the model. Figure 16 shows SHADOZ ozone climatologies from Irene (in South Africa at 25°S), Tahiti (−18.0, −149.0), and La Réunion (−21.1, 55.48) (off Madagascar). Although tropical, these locations are not sufficiently close to the equator to show the characteristic S-shaped profiles of Figure 1. The minimum

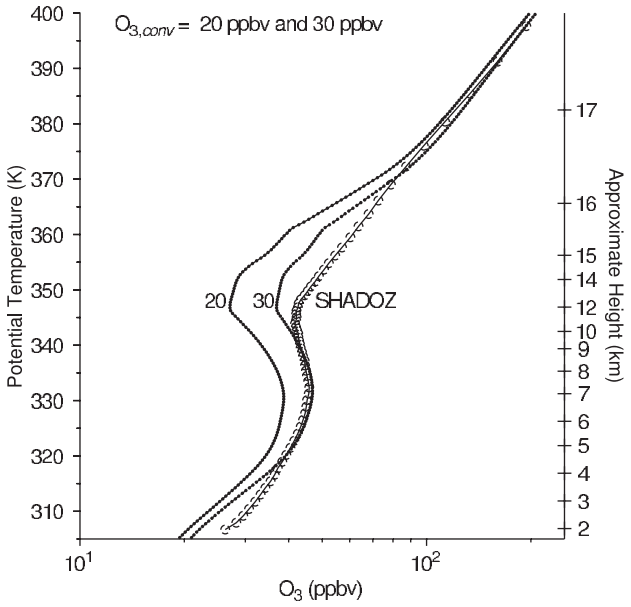

Figure 15. Ozone profiles generated by the model with $O_{3,conv}$ equal to 20 and 30 ppbv, plotted together with the SHADOZ climatology.

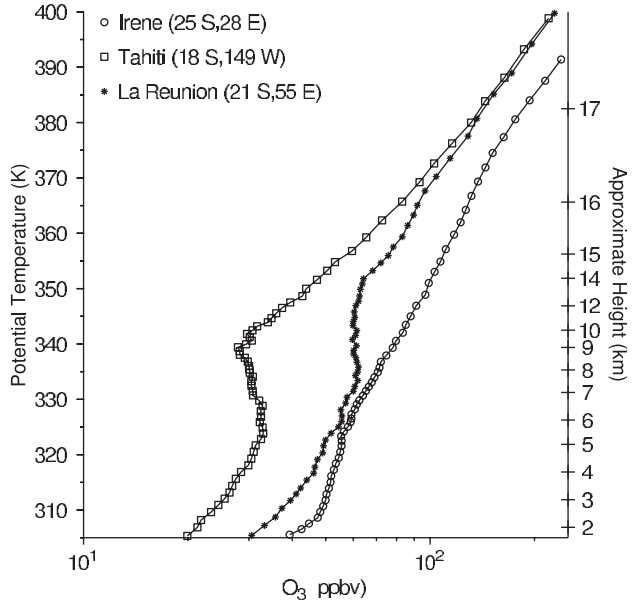

Figure 16. Ozone profiles from three SHADOZ locations, excluded from the SHADOZ climatology for being insufficiently tropical. The Irene profile was obtained from 61 ozonesondes, Tahiti from 75 ozonesondes, and La Réunion from 91 ozonesondes. The latitude and longitude coordinates of each location are shown in parentheses.

at Tahiti lies at 340 K rather than 345 K, while the ozone profiles at Irene and La Réunion show an almost linear increase with potential temperature. Ozone mixing ratios typically increase sharply across the subtropical jet as one goes from the upper tropical troposphere to the lowermost stratosphere [*Folkins and Appenzeller*, 1996], and it is likely that La Réunion and Irene are frequently located on the stratospheric (poleward) side of the jet. Eddy exchange across the jet [e.g., *Postel and Hitchman*, 1999; *Waugh and Polvani*, 2000] may be an important source of ozone to the upper tropical troposphere and may account for some of the differences between the model and the SHADOZ climatology shown in Figure 13.

7. Discussion and Conclusions

[32] The first part of the paper showed that two different indicators (one radiative and the other chemical) gave very similar estimates of the rate of decrease of convective detrainment above 348 K (∼12.5 km). It is important to attempt to diagnose convective detrainment using as many different chemical indicators as possible since each will have different chemical lifetimes and will have affected to varying degrees by exchange with the lowermost stratosphere.

[33] In the second part of the paper we used mass fluxes diagnosed from clear sky radiative heating rates to drive a one-dimensional model of the tropics in which any mass flux divergence was assumed to be balanced by convective detrainment. The virtue of this model is its simplicity. Its only parameter is the mean ozone mixing ratio of air detraining from convective systems, which is reasonably well constrained by observations. Nevertheless, the model

was able to reproduce the S shape common to tropical ozone climatological profiles. This supports the point of view that, to first order, the climatological ozone profile in the tropics can be understood as a sum of vertical advective, convective, and chemical tendencies. The model does, however, produce a deeper and broader 345 K convective ozone minimum than present in the observations. The most likely explanations for this underestimate are (1) that in situ ozone production between 12 and 15 km in the model is too low due to insufficient HO_x precursors such as acetone and CH_3OOH or (2) that eddy transport of ozone across the subtropical jet increases ozone mixing ratios in this region. The data gap between DC-8 (<12 km) and ER-2 altitudes (16–19 km) prevents an accurate assessment of the mean rate of ozone production in the height range over which tropical convective outflow decreases most rapidly. There are also very few simultaneous measurements of meridional wind and ozone mixing ratio in this region, which makes an accurate estimate of the eddy ozone flux $\overline{(v O_3)}$ into the upper tropical troposphere quite difficult.

[34] **Acknowledgments.** Much of this research was done by C.B. as part of his M.S. thesis. Funding for C.B. was provided by the Natural Sciences and Engineering Research Council of Canada under the Global Chemistry and Climate project and by the modeling component of the Atmospheric Chemistry Experiment (ACE). Ozonesonde date were provided through the SHADOZ database archived by J. C. Witte (SMAC at NASA-Goddard), available at http://code916.gsfc.nasa.gov/Data_services/shadoz.

References

Chatfield, R. B., and P. J. Crutzen, Sulfur dioxide in remote oceanic air: Cloud transport of reactive precursors, *J. Geophys. Res.*, *89*, 7111–7132, 1984.

Danielsen, E. F., et al., Meteorological context for fall experiments including distributions of water vapor, ozone, and carbon monoxide, *J. Geophys. Res.*, *92*, 1986–1994, 1987.

Dessler, A. E., The effect of deep, tropical convection on the tropical tropopause layer, *J. Geophys. Res.*, *107*(D3), 10.1029/2001JD000511, 2002.

Dessler, A. E., K. Minschwaner, E. M. Weinstock, E. J. Hinstsa, J. G. Anderson, and J. M. Russell III, The effects of tropical cirrus clouds on the abundance of lower stratospheric ozone, *J. Atmos. Chem.*, *23*, 209–220, 1996.

Folkins, I. A., Origin of lapse rate changes in the upper tropical troposphere, *J. Atmos. Sci.*, *59*, 992–1005, 2002.

Folkins, I. A., and C. Appenzeller, Ozone and potential vorticity at the subtropical tropopause break, *J. Geophys. Res.*, *101*, 18,787–18,792, 1996.

Folkins, I. A., P. O. Wennberg, T. F. Hanisco, J. G. Anderson, and R. J. Salawitch, OH, HO_2, and NO in two biomass burning plumes: Sources of HO_x and implications for ozone production, *Geophys. Res. Lett.*, *24*, 3185–3188, 1997.

Folkins, I. A., R. Chatfield, H. Singh, Y. Chen, and B. Heikes, Ozone production efficiencies of acetone and peroxides in the upper troposphere, *Geophys. Res. Lett.*, *25*, 1305–1308, 1998.

Folkins, I. A., M. Loewenstein, J. Podolske, S. Oltmans, and M. Proffitt, A barrier to vertical mixing at 14 km in the tropics: Evidence from ozonesondes and aircraft measurements, *J. Geophys. Res.*, *104*, 22,095–22,101, 1999.

Folkins, I. A., S. J. Oltmans, and A. Thompson, A relationship between convective outflow and surface equivalent potential temperatures in the tropics, *Geophys. Res. Lett.*, *27*, 2549–2552, 2000.

Fu, Q., and K. N. Liou, On the correlated *k*-distribution method for radiative transfer in nonhomogeneous atmospheres, *J. Atmos. Sci.*, *49*, 2139–2156, 1992.

Fujiwara, M., K. Kita, and T. Ogawa, Stratosphere-troposphere exchange of ozone associated with the equatorial Kelvin wave as observed with ozonesondes and rawinsondes, *J. Geophys. Res.*, *103*, 19,173–19,182, 1998.

Gettelman, A., M. L. Salby, and F. Sassi, The distribution and influence of convection in the tropical tropopause region, *J. Geophys. Res.*, *107*, 10.1029/2001001048, in press, 2002.

Jacob, D. J., et al., Origin of ozone and NO_x in the tropical troposphere: A photochemical analysis of aircraft observations over the South Atlantic basin, *J. Geophys. Res.*, *101*, 24,235–24,250, 1996.

Jaeglé, L., et al., Observed OH and HO_2 in the upper troposphere suggest a major source from convective injection of peroxides, *Geophys. Res. Lett.*, *24*, 3181–3184, 1997.

Lacis, A. A., D. J. Wuebbles, and J. A. Logan, Radiative forcing of climate by changes in the vertical distribution of ozone, *J. Geophys. Res.*, *95*, 9971–9982, 1990.

Lelieveld, J., et al., The Indian Ocean Experiment: Widespread air pollution from south and southeast Asia, *Science*, *291*, 1031–1036, 2001.

Logan, J. A., An analysis of ozonesonde data for the troposphere: Recommendations for testing 3-D models and development of a gridded climatology for tropospheric ozone, *J. Geophys. Res.*, *104*, 16,115–16,149, 1999.

McKeen, S. A., et al., The photochemistry of acetone in the upper troposphere: A source of odd-hydrogen radicals, *Geophys. Res. Lett.*, *24*, 3177–3180, 1997.

Postel, G. A., and M. H. Hitchman, A climatology of Rossby wave breaking along the subtropical tropopause, *J. Atmos. Sci.*, *56*, 359–373, 1999.

Prather, M. J., and D. J. Jacob, A persistent imbalance in HO_x and NO_x photochemistry of the upper troposphere driven by deep tropical convection, *Geophys. Res. Lett.*, *24*, 3189–3192, 1997.

Schultz, M. G., et al., On the origin of tropospheric ozone and NO_x over the tropical South Pacific, *J. Geophys. Res.*, *104*, 5829–5843, 1999.

Sherwood, S. C., and A. E. Dessler, A model for transport across the tropical tropopause, *J. Atmos. Sci.*, *58*, 765–779, 2001.

Singh, H. B., M. Kanakidou, P. J. Crutzen, and D. J. Jacob, High concentration and photochemical fate of oxygenated hydrocarbons in the global troposphere, *Nature*, *378*, 50–54, 1995.

Thompson, A. M., et al., Ozone observations and a model of marine boundary layer photochemistry during SAGA 3, *J. Geophys. Res.*, *98*, 16,955–16,968, 1993.

Thompson, A. M., et al., The 1998–2000 Southern Hemisphere Additional Ozonesondes (SHADOZ) tropical ozone climatology: Comparisons with TOMS and ground-based measurements, *J. Geophys. Res.*, *107*, 10.1029/2001JD000967, in press, 2002.

Tuck, A. F., et al., The Brewer Dobson circulation in the light of high altitude in situ aircraft observations, *Q. J. R. Meteorol. Soc.*, *124*, 1–70, 1997.

Waugh, D. W., and L. M. Polvani, Climatology of Intrusions into the tropical upper troposphere, *Geophys. Res. Lett.*, *27*, 3857–3860, 2000.

Wennberg, P. O., et al., Hydrogen radicals, nitrogen radicals, and the production of ozone in the upper troposphere, *Science*, *279*, 49–53, 1998.

Yanai, M., S. Esbensen, and J. Chu, Determination of bulk properties of tropical cloud clusters from large-scale heat and moisture budgets, *J. Atmos. Sci.*, *30*, 611–627, 1973.

C. Braun and I. Folkins, Department of Oceanography, Dalhousie University, Halifax, Nova Scotia, B3H 4J1, Canada. (cbraun@atm.dal.ca; Ian.Folkins@dal.ca)

A. M. Thompson and J. C. Witte, NASA-Goddard Space Flight Center, Atmospheric Chemistry and Dynamics Branch, Code 916, Greenbelt, MD 20771, USA. (thompson@gator1.gsfc.nasa.gov; witte@gavial.gsfc.nasa.gov)